Auxiliary material for:

Simulating maar-diatreme volcanic systems in bench-scale experiments

R.G. Andrews[1], J.D.L. White1, T. Dürig[2], B. Zimanowski[3]

r.c.andrews@btinternet.com

1 – Department of Geology, University of Otago, Dunedin, New Zealand

2 – Institute of Earth Sciences, University of Iceland, Iceland

3 – Physikalisch-Vulkanologisches Labor, Universität Würzburg, Würzburg, Germany

Introduction

The data files present here consist of five video files of the key experimental runs featured in the paper.

The video files are vital for understanding the data and conclusions present in the paper, but for obvious technical reasons need to be included as digital-only supplements.

In addition, 12 image files are presented here as auxiliary figures, as are 3 tables.

Auxiliary Videos

(ms1) Video 1 | High-speed (originally 1000 fps, now 60 fps) footage of Run 21, first depicted in Fig. 1. 16 cm blast depth, 1.5 MPa initial pressure.

(ms2) Video 2 | High-speed (originally 1000 fps, now 60 fps) footage of Run 22, first depicted in Fig. 3. 8 cm blast depth, 1.5 MPa initial pressure.

(ms3) Video 3 | High-speed (originally 1000 fps, now 60 fps) footage of Run 10, first depicted in Fig. 4. 24 cm blast depth, 2 MPa initial pressure.

(ms4) Video 4 | High-speed (originally 1000 fps, now 60 fps) footage of Run 20, first depicted in Fig. 8. 24 cm blast depth, 1.5MPa initial pressure.

(ms5) Video 5 | High-speed (originally 1000 fps, now 30 fps) footage of Run 19, first depicted in Fig. 8. 24 cm blast depth, 2 MPa initial pressure.

Auxiliary Figures

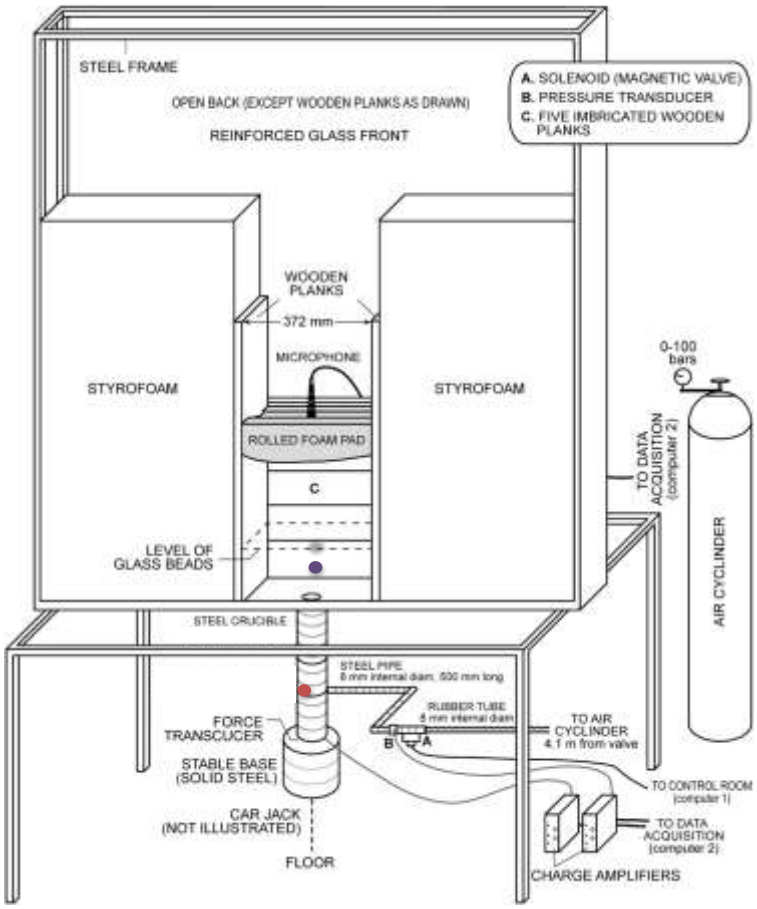

Figure S1 | A diagrammatical representation of the experimental set up used in these runs, (after Ross et al., 2008b). The addition to the previous set-up of a pressure sensor and a force transducer inside the crucible (red circle), additional pressure sensors SIKA 1 (purple circle) & 2 (blue circle) in the back wall of the apparatus, are shown. Runs were grouped together based on the initial pressure of the compressed argon gas (0.5 MPa, 1 MPa, 1.5 MPa, and 2 MPa), in order of either three ascending runs from deep to shallow crucible depths, three descending runs from shallow to deep crucible depths, or single runs.

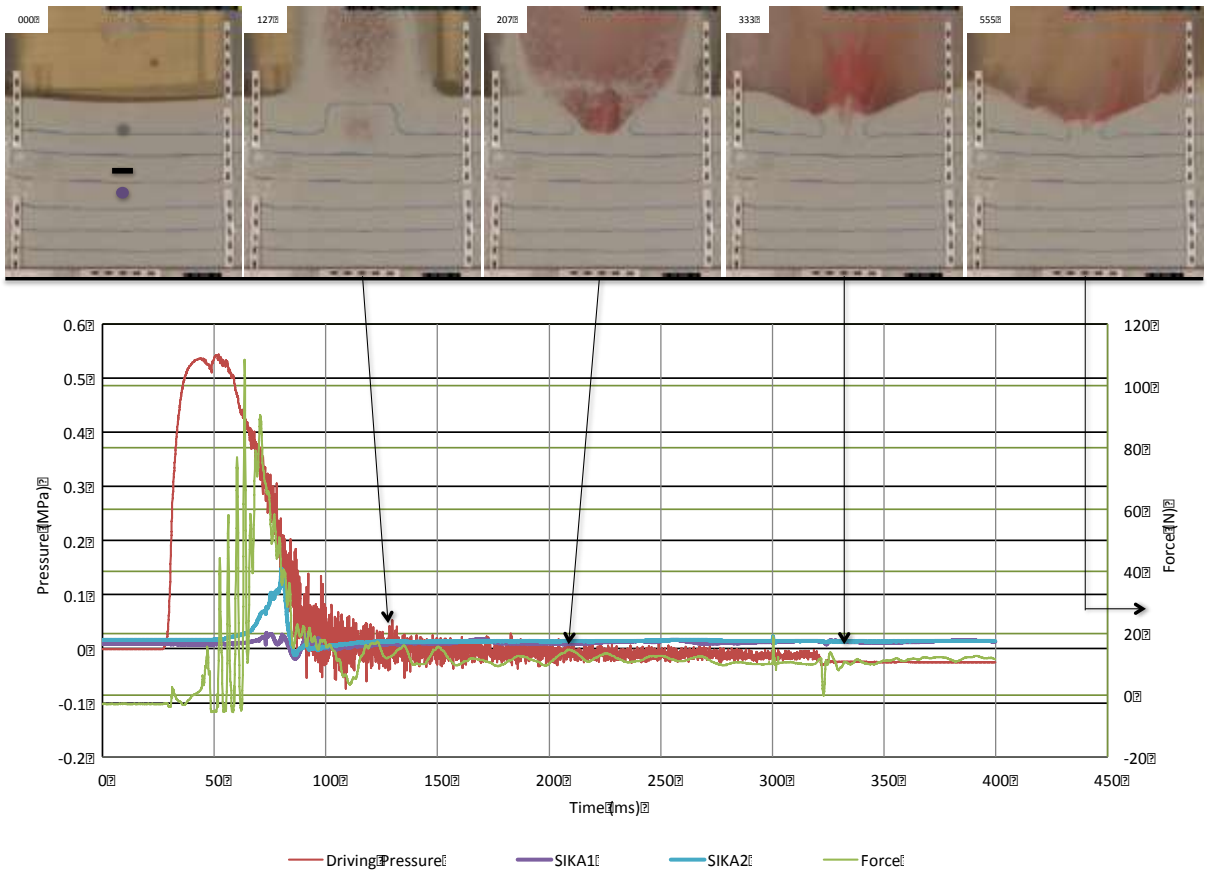

Figure S2 | Driving pressures and force record for Run 17. The driving pressure sensor located within the crucible opposite the gas line, and the force transducer below the crucible. SIKA 1 and 2 are pressure sensors located behind the host white bead mass, which was in contact with them; this is why their initial pressure readings are slightly above 0 MPa. The pressure peaks observed for each sensor are in accordance with the timing of the expanding gas cavity's propagation as it moved through the crucible, then upwards, coming into contact with SIKA 2; SIKA 1 is below the cavity in this run. For the pressure and force curves beyond the initial declines, the sensors are only registering system resonance. At the pressure (including SIKA 2) and force peaks, the only the beginnings of the surface and viewing wall deformaiton are observed. As the t=127 ms frame demonstrates, the cavity as an inverted cone shape is visible at 67 ms after the pressure peak is recorded – indicating there is a lag time between the pressure peak registering on the pressure sensors and the displacement of the beads.

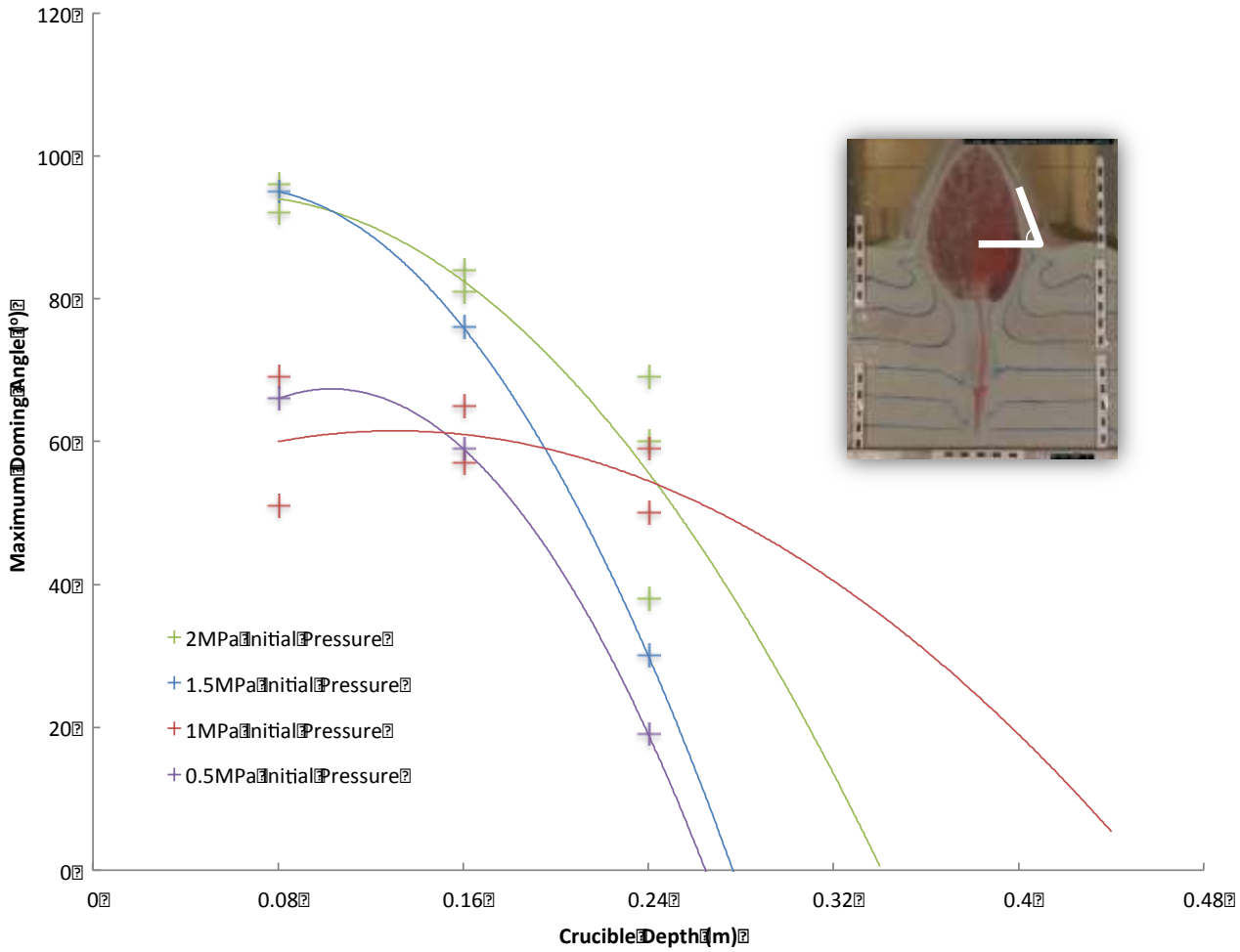

Figure S3 | Crucible Depth v Maximum Doming Angle for all runs in this study. The maximum doming angle was measured at the outer edge of the dome. Angles were measured from the centre of the dome outwards towards the peripheries until collapse began to occur (white lines, inset frame). Zero degrees = horizontal plane to the bead mass surface. Approximate trend lines for each initial pressure set are shown.

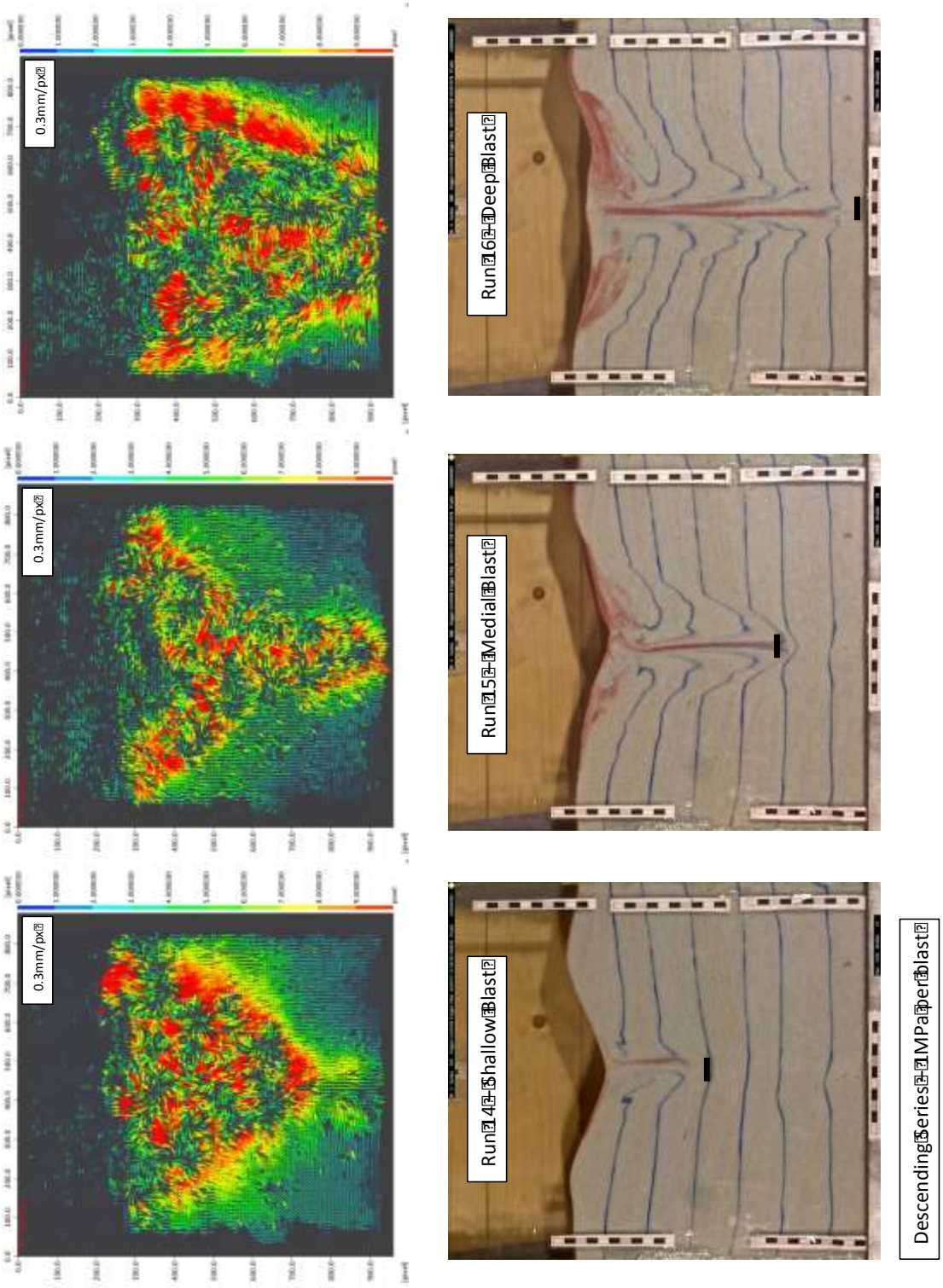

Figure S4 | Particle Image Velocimetry (PIV) analyses for a descending 1 MPa blast series {JPIV® open-source software}. The three lower frames show the post-shot craters and diatreme deposits for each successive run. The PIV-calculated displacements depict the overall displacements from t=0 ms to the final post shot crater (at t=900 ms) at the end of each run; thus, the time-averaged transient craters are modelled for each run.

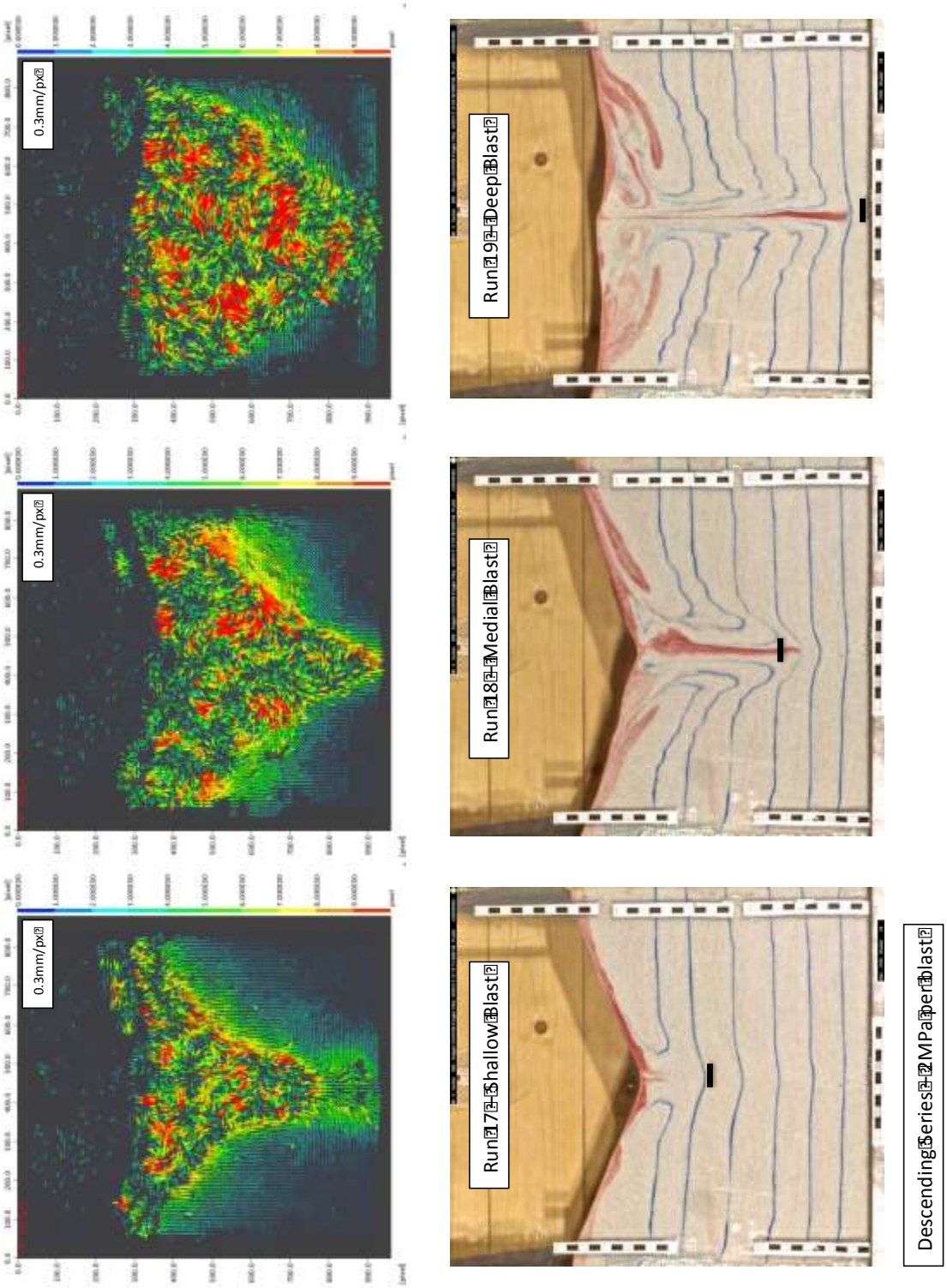

Figure S5 | Particle Image Velocimetry (PIV) analyses for a descending 2 MPa blast series {JPIV® open-source software}. The three lower frames show the post-shot craters and diatreme deposits for each successive run.

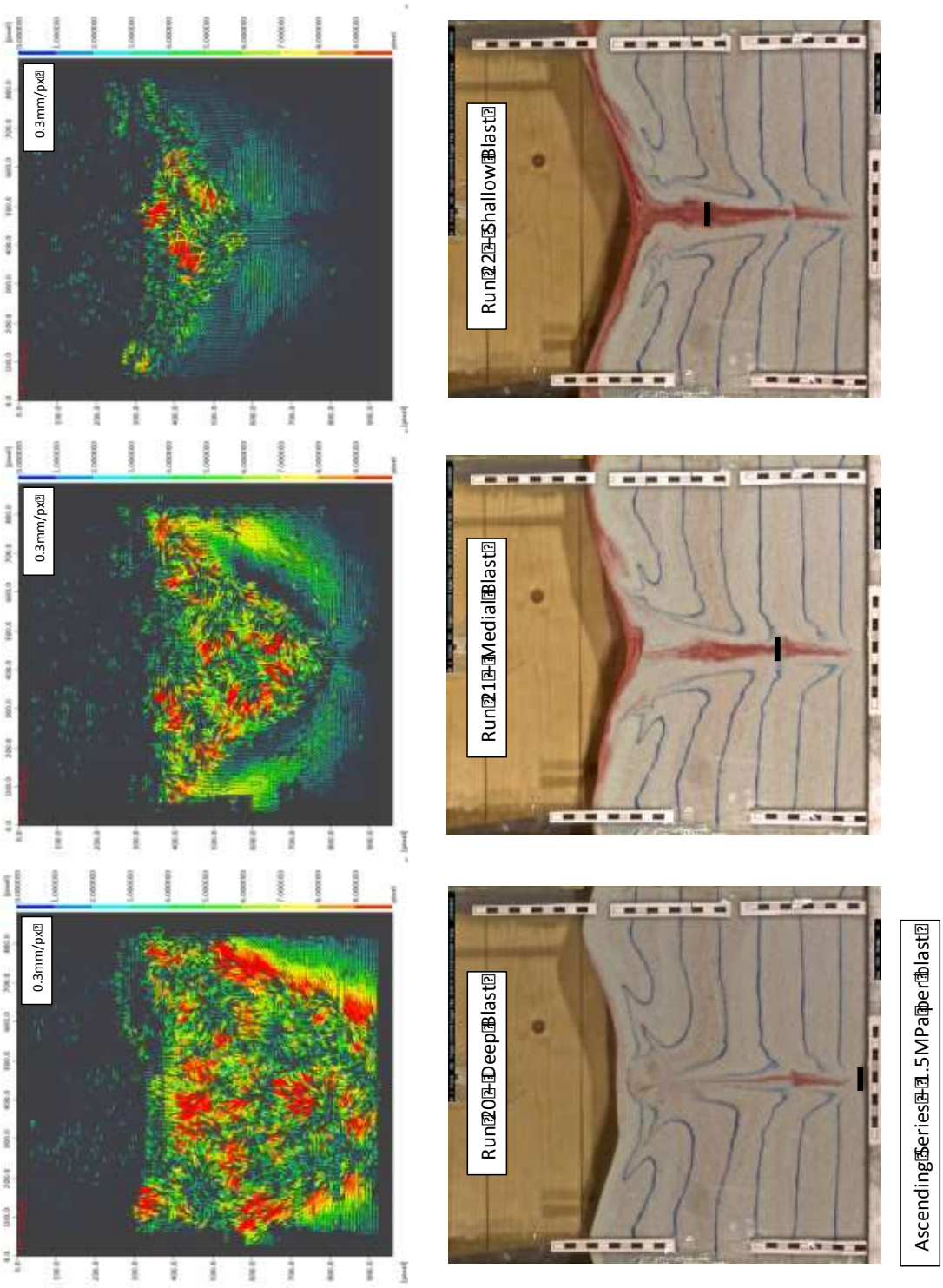

Figure S6 | Particle Image Velocimetry (PIV) analyses for an ascending 1.5 MPa blast series {JPIV® open-source software}. The three lower frames show the post-shot craters and diatreme deposits for each successive run.

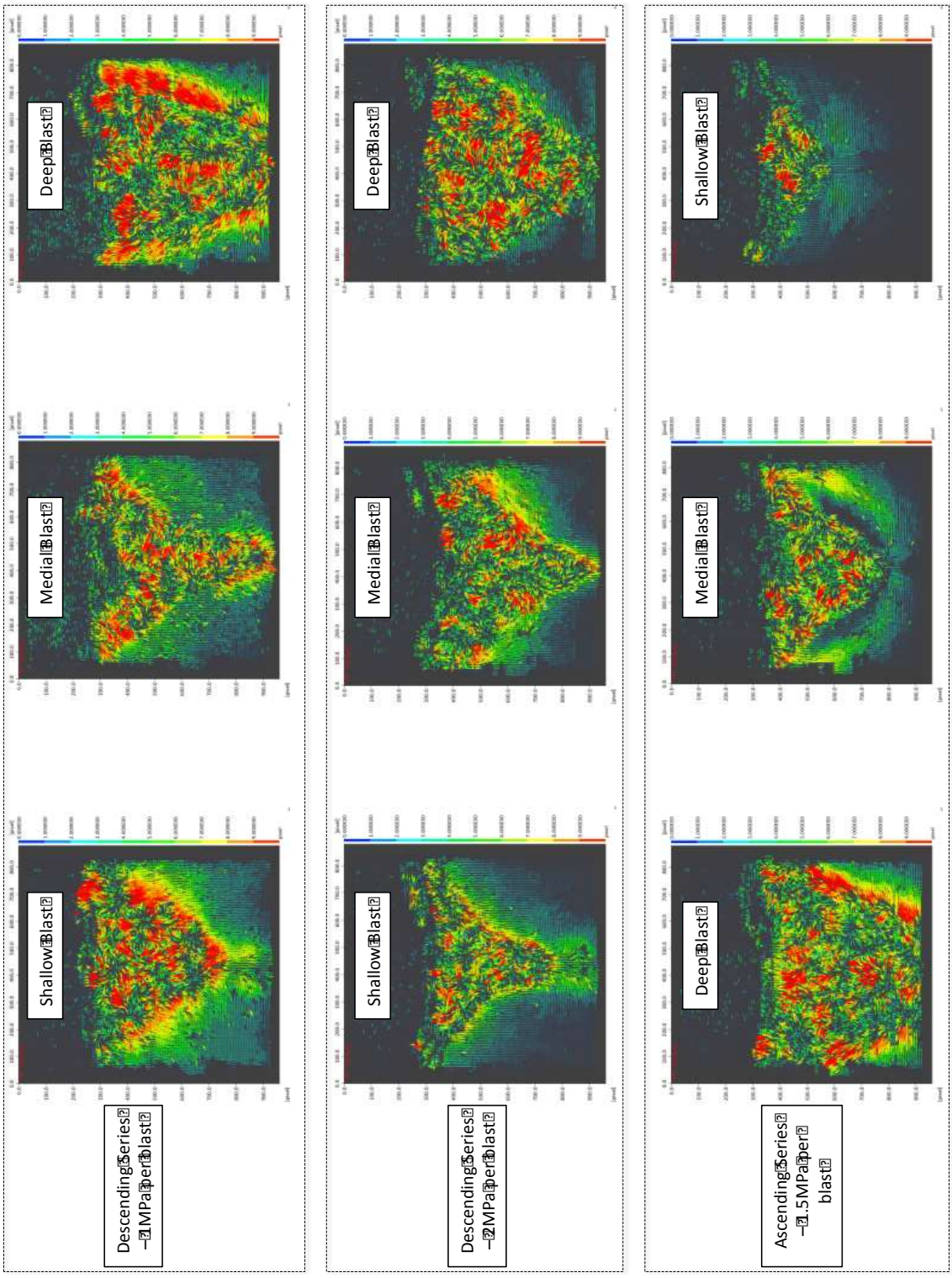

Figure S7 | Particle Image Velocimetry (PIV) analyses for two descending blast series (1, 2 MPA) and one ascending blast series (1.5 MPa) {JPIV® open-source software}. Due to time constraints, no ascending blast series of 1 or 2 MPa initial pressures were conducted; thus, a comparison of the 1.5 MPa ascending series with two descending blast series with initial pressures of +/- 33% is made.

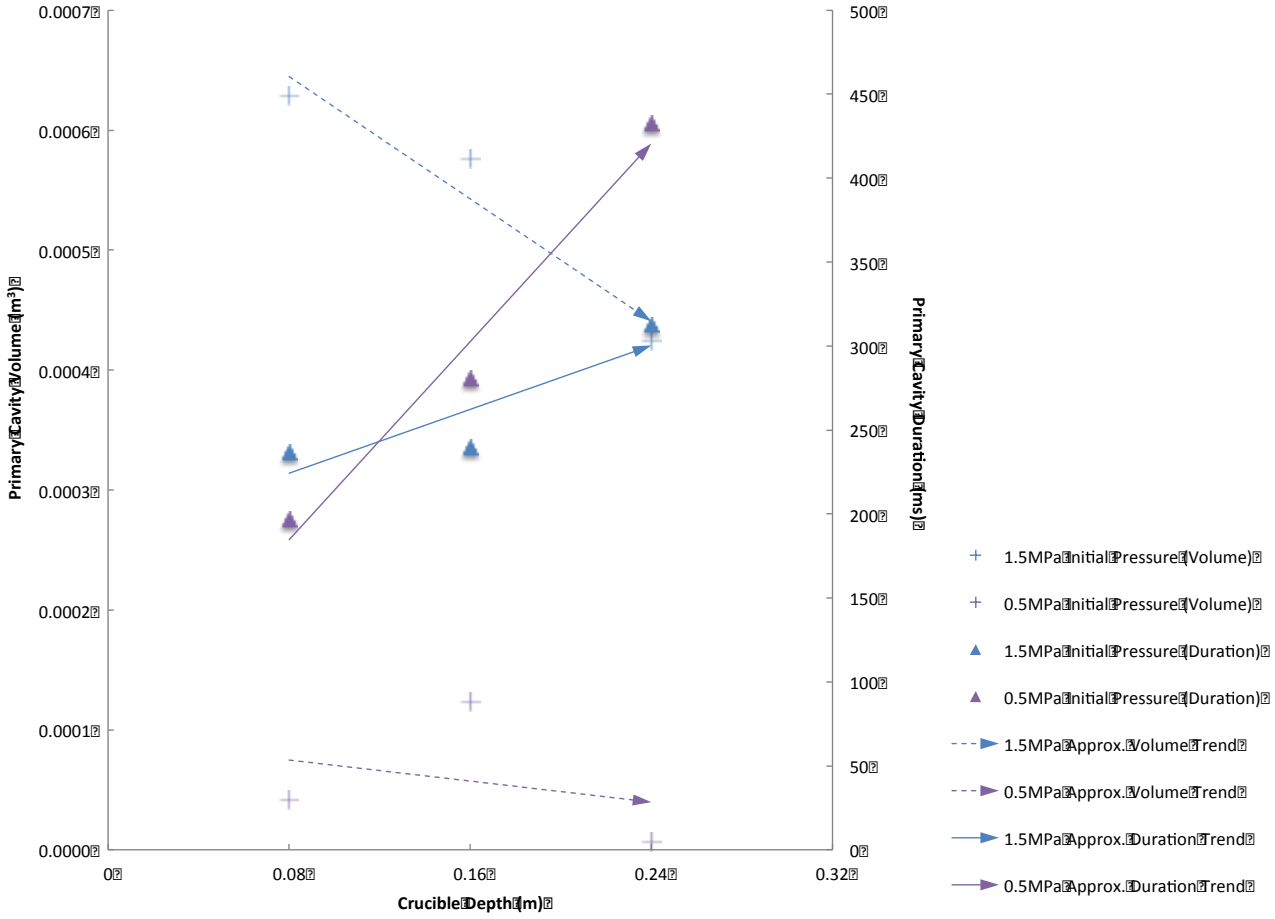

Figure S8 | Crucible Depth v Primary Cavity Volume & Duration for 0.5 & 1.5 MPa initial pressures.

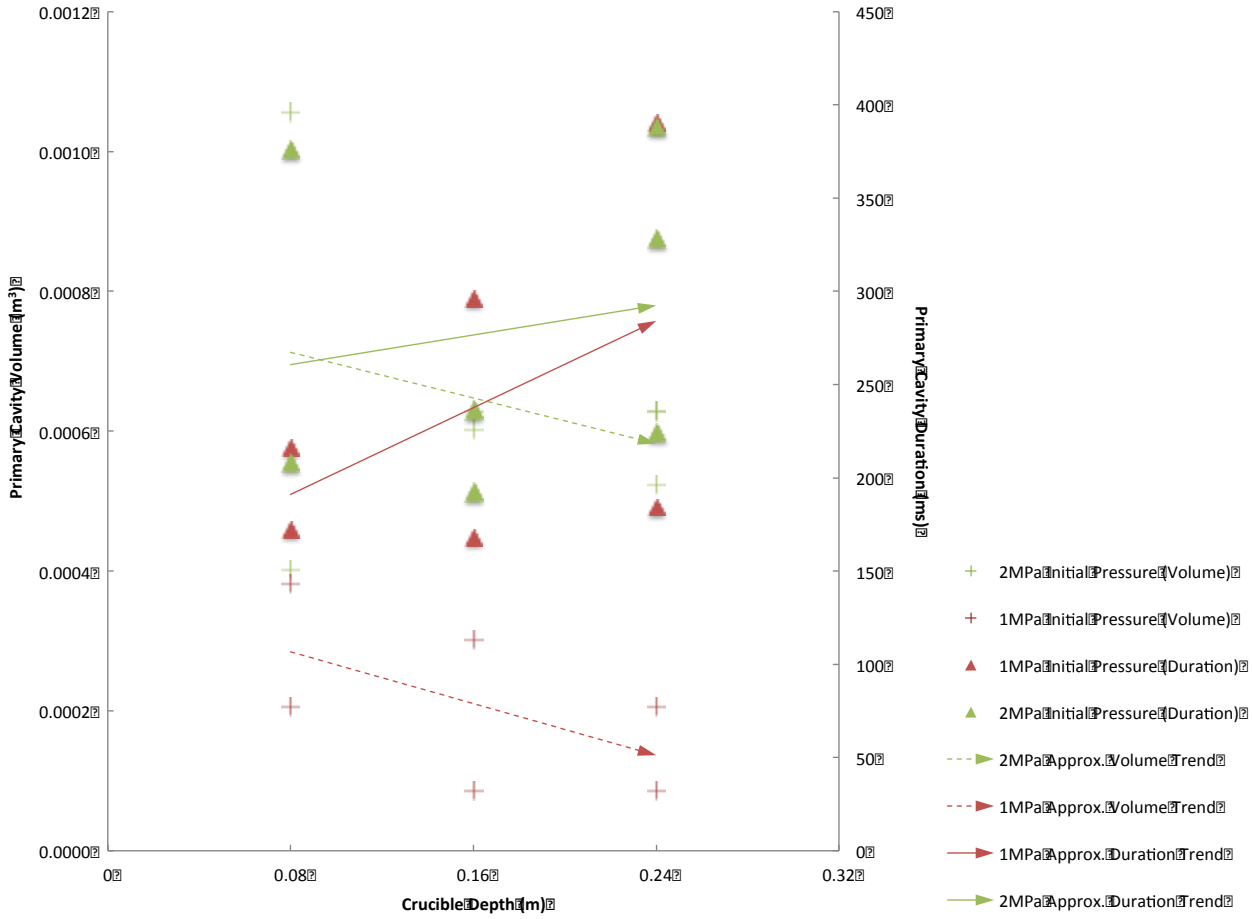

Figure S9 | Crucible Depth v Primary Cavity Volume & Duration for 1 & 2 MPa initial pressures.

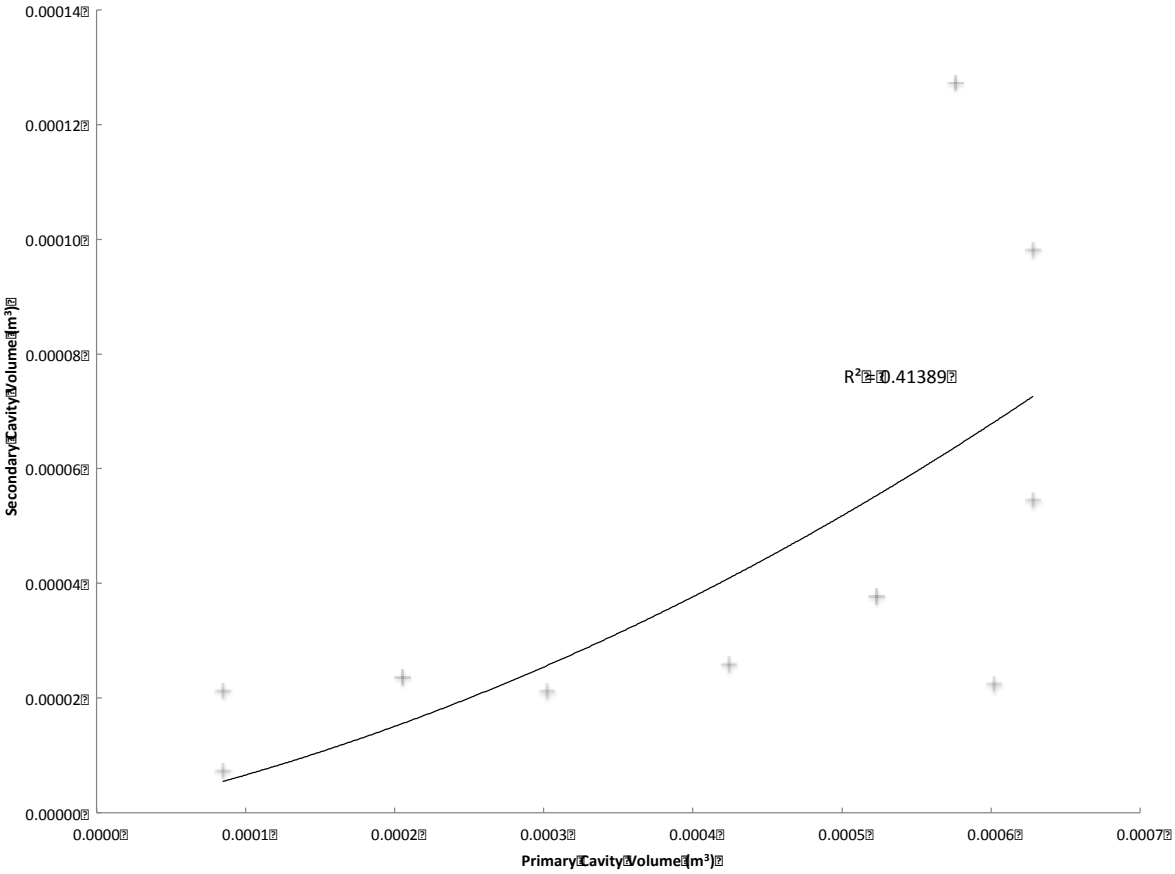

Figure S10 | Primary Cavity Volume v Secondary Cavity Volume for all runs used in this study. The R^2 value for the approximate trend line is shown.

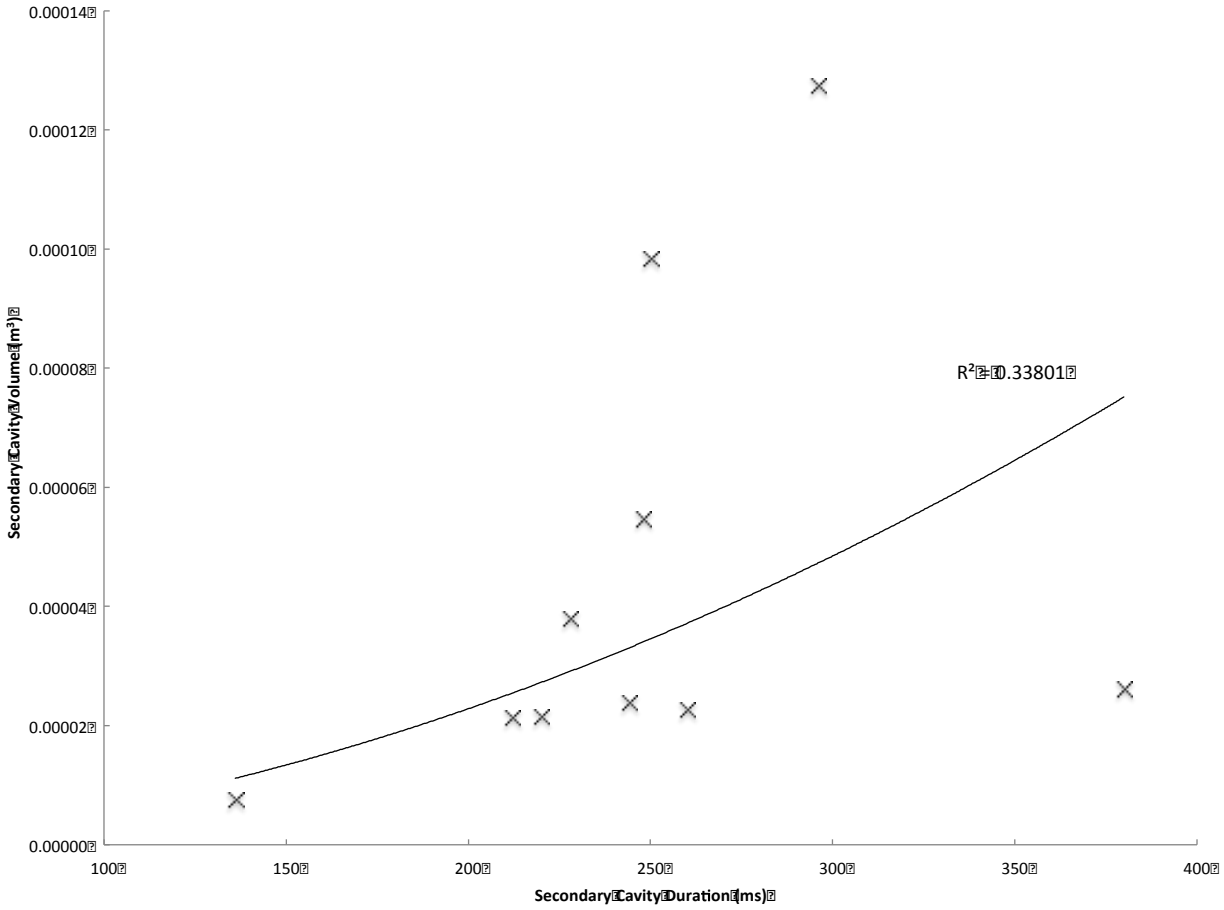

Figure S11 | Secondary Cavity Duration v Secondary Cavity Volume for all runs used in this study. The R^2 value for the approximate trend line is shown.

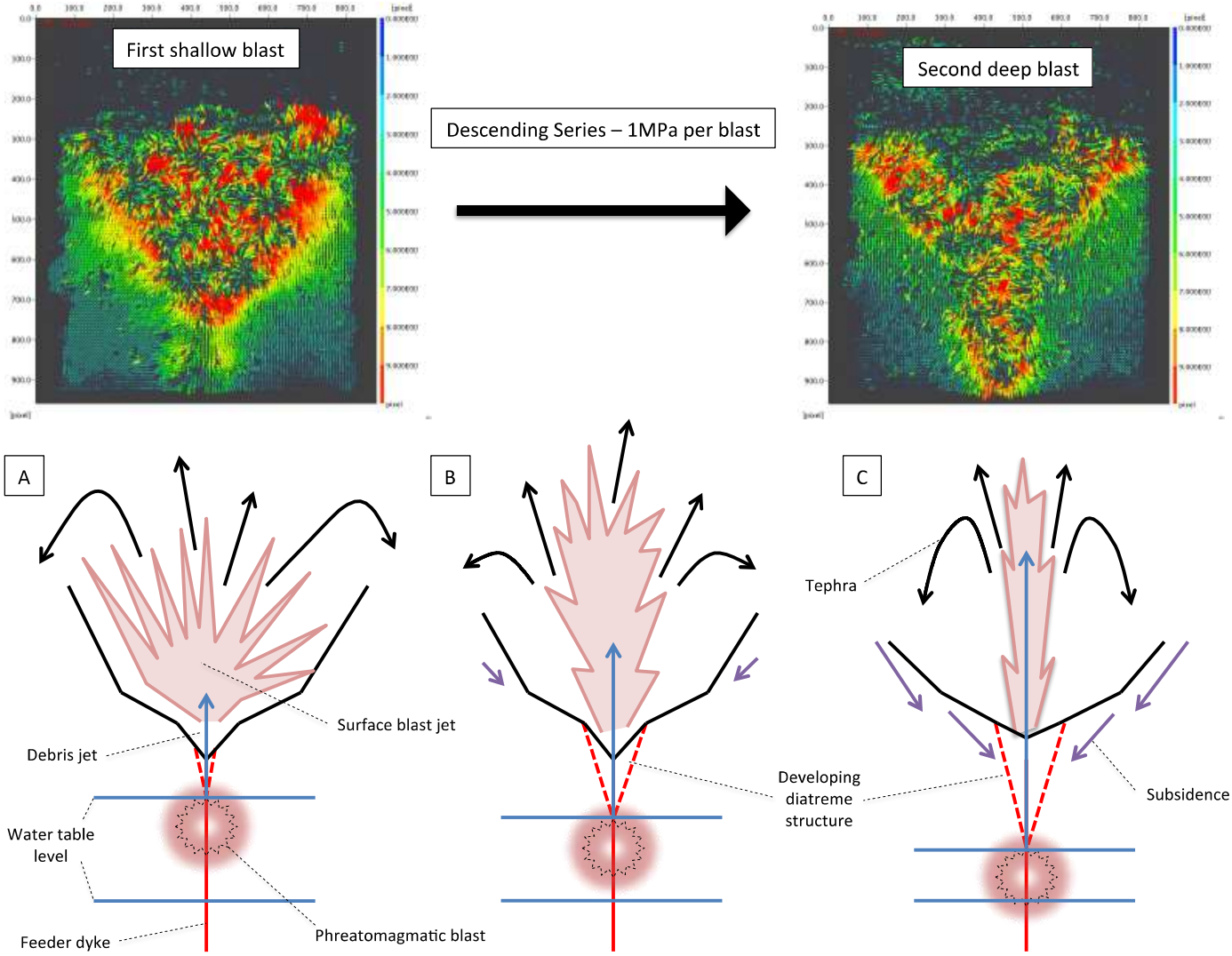

Figure S12 | A schematic illustration (bottom) of the evolution of a maar-diatreme system with a deepening blast series, as depicted by the accompanying PIV images (top). **A** depicts an initial, large explosion generating a sizeable crater, which is then modified and flatted in **B** as a deepening series of phreatomagmatic blasts – which tracks the water table – vertically focuses the ejection of debris, causing a higher proportion to fall back into the transient crater as the eruption progresses. Syn- and post-eruption subsidence contribute to the flattening of the crater in **C**.

Run Number	Crucible opening depth below overlying stratigraphy (m)	Initial Pressure (MPa)	Doming Base Diameter (m)[b]	Maximum doming angle from horizontal (°)[c]
5[d]	**0.08**	**1**	**0.175**	**69**
6	0.16	1	0.170	65
7	0.24	1	0.155	50
8	**0.08**	**2**	**0.230**	**92**
9	0.16	2	0.205	81
10	0.24	2	0.180	69
11	**0.08**	**0.5**	**0.145**	**66**
12	0.16	0.5	0.130	59
13	0.24	0.5	0.100	19
14	**0.08**	**1**	**0.175**	**51**
15	0.16	1	0.135	57
16	0.24	1	0.150	59
17	**0.08**	**2**	**0.210**	**96**
18	0.16	2	0.205	84
19	0.24	2	0.200	60
20	**0.24**	**1.5**	**0.200**	**30**
21	0.16	1.5	0.175	76
22	0.08	1.5	0.205	95
23[e]	**0.24**	**2**	**0.215**	**38**

[a]Runs used in this paper involved a constant red bead mass (68g) and pressurised gas release time (300ms).

[b]Approximate distance between the dome's outer lateral edges prior to collapse.

[c]Measured from the center of the dome outwards to the peripheries until collapse occurs.

[d]First crater-forming blasts in a series of successive runs are shown in bold.

[e]This run used a paper diaphragm to cover the orifice within the crucible instead of a rubber valve.

Table S1 | Selected experimental runs with associated doming phenomenology[a]. Early runs were tests of the experimental system; later runs featured variations to the system not addressed here. Runs 1-4 were test runs using vastly longer valve opening times and different bead mass set-ups, in order to test the pressure and force sensors, and the recording equipment.

Table S2 | Selected experimental runs with associated volume data for the generated craters[a].

Run Number	Crucible opening depth below overlying stratigraphy (m)	Initial Pressure (MPa)	Crater Diameter (m)	Crater Depth (m)	Diameter/Depth ratio	Crater Volume (m^3)[b]
5[c]	**0.08**	**1**	**0.078**	**0.011**	**7.100**	**0.000018**
6	0.16	1	0.075	0.023	3.261	0.000034
7	0.24	1	0.100	0.035	2.857	0.000092
8	**0.08**	**2**	**0.131**	**0.040**	**3.275**	**0.000180**
9	0.16	2	0.131	0.025	5.240	0.000112
10	0.24	2	0.131	0.010	13.100	0.000045
11	**0.08**	**0.5**	**0.047**	**0.011**	**4.264**	**0.000006**
12	0.16	0.5	0.075	0.009	8.333	0.000013
13	0.24	0.5	0.075	0.023	3.261	0.000034
14	**0.08**	**1**	**0.078**	**0.029**	**2.693**	**0.000046**
15	0.16	1	0.081	0.009	9.028	0.000016
16	0.24	1	0.100	0.006	16.667	0.000016
17	**0.08**	**2**	**0.138**	**0.050**	**2.760**	**0.000249**
18	0.16	2	0.141	0.024	5.875	0.000125
19	0.24	2	0.141	0.011	12.818	0.000057
20	**0.24**	**1.5**	**0.113**	**0.028**	**4.036**	**0.000094**
21	0.16	1.5	0.116	0.029	4.000	0.000102
22	0.08	1.5	0.125	0.044	2.841	0.000180
23[e]	**0.24**	**2**	**0.150**	**0.045**	**3.333**	**0.000265**

[a]Runs used in this paper involved a constant red bead mass (68g) and pressurised gas release time (300ms).

[b]Calculations for the approximate volume of the crater treats the crater morphology as a cone.

[c]First crater-forming blasts in a series of successive runs are shown in bold.

Run Number	Crucible opening depth below overlying stratigraphy (m)	Initial Pressure (MPa)	Approximate volume of primary cavity (m^3)[b]	Primary cavity duration (ms)[c]	Approximate volume of secondary cavity (m^3)[de]	Secondary cavity duration (ms)[c]
5[f]	**0.08**	**1**	**0.000381**	**216**	-	-
6	0.16	1	0.000302	296	0.000021	212
7	0.24	1	0.000205	390	0.000024	244
8	**0.08**	**2**	**0.000402**	**192**	-	-
9	0.16	2	0.000602	224	0.000038	228
10	0.24	2	0.000523	388	0.000022	260
11	**0.08**	**0.5**	**0.000042**	**196**	-	-
12	0.16	0.5	0.000123	280	-	-
13	0.24	0.5	0.000007	432	-	-
14	**0.08**	**1**	**0.000205**	**172**	-	-
15	0.16	1	0.000085	168	0.000021	220
16	0.24	1	0.000085	184	0.000007	136
17	**0.08**	**2**	**0.001056**	**208**	-	-
18	0.16	2	0.000628	236	0.000054	248
19	0.24	2	0.000628	328	0.000098	250
20	**0.24**	**1.5**	**0.000424**	**312**	0.000026	**380**
21	0.16	1.5	0.000576	239	0.000127	296
22	0.08	1.5	0.000628	236	-	-
23	**0.24**	**2**	**0.000628**	**376**	-	-

[a]Runs used in this paper involved a constant red bead mass (68g) and pressurised gas release time (300ms).

[b]Calculations for the approximate volume of the cavity treats the cavity morphology as an inverted teardrop shape, comprised of a half-sphere and a cone.

[c]Duration time measured between first observed gas cavity form through white bead deformation (opening), and closure by zipping.

[d]Calculations for the approximate volume of the secondary cavity treats the cavity morphology as a teardrop shape, comprised of a half-sphere and a cone.

[e]Only largest secondary cavity is included. Not all runs have secondary cavities.

[f]First crater-forming blasts in a series of successive runs are shown in bold.

Table S3 | Selected experimental runs with associated volume and duration data for the primary and secondary cavities[a].